Hindawi
Advances in Civil Engineering
Volume 2022, Article ID 7034778, 16 pages
https://doi.org/10.1155/2022/7034778

Research Article

Impact of Seepage on the Underground Water Level in a Complex Soil-Water-Structure System

Youfeng Li,[1,2] Linlong Mu ,[3,4] and Jie Cao [1,2]

[1]*Shaanxi Key Laboratory for the Property and Treatment of Special Soil and Rock, Xi'an, Shaanxi 710043, China*
[2]*China Jikan Research Institute of Engineering Investigation and Design Co. Ltd., Shaanxi 710000, China*
[3]*Department of Geotechnical Engineering, Tongji University, Shanghai 200092, China*
[4]*Key Laboratory of Geotechnical and Underground Engineering of Ministry of Education, Tongji University, Shanghai 200092, China*

Correspondence should be addressed to Linlong Mu; mulinlong@tongji.edu.cn

Received 13 September 2022; Revised 9 November 2022; Accepted 10 November 2022; Published 6 December 2022

Academic Editor: Jian Zhang

The antifloating design of underground structures is very important in areas with high underground water levels, and reasonable evaluation of the buoyancy is based on accurately describing the distribution of the groundwater level. However, the natural groundwater flow would be disturbed by the structure, which is not considered in the antifloating design. In the present paper, the influence of the width of an underground structure on the groundwater level in homogeneous soil is investigated through an indoor physical model test in the first place, which serves as a benchmark for the numerical simulation. Then, the parametrical study is carried out with numerical simulation. The results show that the width of the structure has the greatest influence on the water level around the structure, followed by the influence of the insertion depth, whereas the length has little influence. The hydraulic gradient has a significant effect on that as well. Moreover, the hydraulic conductivity ratio between different soil layers also affects the water level magnitude. Based on the results, a prediction method for the groundwater level around the structure for both homogeneous soil and multilayer soil has been developed and evaluated.

1. Introduction

With the growth of the social economy, increasing numbers of underground infrastructures are being constructed [1–3]. Many of the structures have been constructed in areas under poor geotechnical conditions, such as subsoil mainly consisting of soft deposits with a high groundwater level and a large thickness of aquifers [4–6]. They are generally exposed to high buoyancy forces, which may uplift the underground structure. Therefore, the reasonable antifloating design of the underground structure is one of the most important projects in these areas [7–9].

At present, the most commonly used method for the calculation of the buoyancy acting on the structure is based on the classical Archimedes' principle and a further reduction is generally given when considering the soil properties [9, 10]. Therefore, a reasonable prediction of the underground water level is the premise of the accurate buoyancy calculation. However, the underground water is generally dynamically flowing; it is in a steady-state flow before the construction of the underground structure. When an impervious underground structure intersects aquifers, the natural groundwater flow pattern will be modified because the underground structure reduces the aquifer section totally or partially, forming a "barrier" to the water flow, and obstructing the water flow in terms of both rate and direction [11–13]. This effect can be divided into two types: the effect produced during the construction period and that produced after the construction. Many research studies has been carried out to investigate the effect produced during the construction period [14–17], however, this effect is generally local and unstable, moreover, it also has little influence on the buoyancy of the structure. Considering the long-term impact, it is in a steady state before disturbance and achieves

another steady state after disturbance when the underground structure is constructed [18]. This will result in an increment of the water level along the side of the structure (upstream side) and a decrement on the other side (downstream side) [19], and a water pressure difference acting on both sides of the structure is produced [20], which would result in the variation of the buoyancy. However, the effect of this is not considered in the antifloating design of the engineering practice.

The hydraulic head variation produced by the barrier effect can be expressed mathematically as the difference between the undisturbed hydraulic gradient and the hydraulic gradient once the underground structure is constructed [20]. The magnitude of this variation is proportional to the natural groundwater gradient perpendicular to the construction [21, 22], it would be enormous in the area where the regional hydraulic gradient is relatively larger, especially in some coastal region cities, for example, an approximation of 15% of the regional hydraulic gradient is reported for Hong Kang in China [23], Marinos and Kavvadas [24] concluded that for a range of hydraulic gradients from 10 to 15%, when the tunnel is located below the groundwater surface, the head rise generated cover a zone defined by 35–55% of the tunnel's height. Moreover, the barrier effect is also related to the structure geometry (i.e., insertion depth and width) [25–28], and aquifer soil characteristics (i.e., aquifer permeability coefficient and aquifer thickness) [29, 30]. However, in most of the studies, the problem is simplified to a 2D problem [31, 32], or in 3D numerical simulations, but the structure is extended to the boundary along the direction perpendicular to the flow direction [27], this can be called quasi-2D, which induces an overestimation of the barrier effect generated by a local impervious structure [33], most importantly, moly the average or maximum magnitude of the water level variation is generally provided considering different structure geometry [14, 20, 34, 35]. However, there is little literature on the nonuniform distribution of groundwater level around the structure, and no simplified calculation method of which can be founded in the previous research for neither homogeneous nor multilayer soil.

Therefore, in the present paper, seepage model tests with different underground structure geometries are carried out to study the influence of seepage on the nonuniform distribution of the water level and pore water pressure around the underground structure. Through the calculation of a three-dimensional finite element model, the distribution of the seepage field under a series of different working conditions is studied, and a modified formula for the water level around the structure is established. Furthermore, the results are extended to multilayer soil, and a simplified calculation method for multilayer soil is proposed.

2. Model Test

2.1. Test Equipment. Figure 1 shows the schematic of the model test system, which includes a test tank, an underground structure, a water supply system, and a monitoring system. The test tank is made of a steel frame and polymethyl methacrylate (PMMA), 1.5 m in length, 1.0 m in width, and 1.5 m in height, and the wall thickness of the tank is 20 mm. Some angle irons are welded to the outside of the box to prevent excessive deformation; the tank is designed to meet the water tightness requirement. A circulating water circuit and an overflow water supply device are adopted in the water supply system to ensure that the water level in the water supply tank remains stable. Drainage pipes, which have diameters of 25 mm, with valves are arranged on both sides of the tank; the layout is shown in Figure 1. To prevent the water from flowing along the sidewall of the box, the drainage pipes should be required to penetrate into the tank. Some space is needed to do the operations that install the pipes onto the tank and cover the pipes, thus the pipes penetrate 100 mm into the tank. Thus, the seepage boundary starts and ends from the outlet of the pipes, that is, from 0.1 m to 1.4 m. And the geotextile covers the pipes to prevent sand particles from being washed away by the water through the holes of the pipes.

2.2. Underground Structure Model and Soil Properties. Three cuboid underground structure models are made with PMMA; the model dimensions are 200 mm × 200 mm × 450 mm, 200 mm × 300 mm × 450 mm, and 200 mm × 400 mm × 450 mm (length (l) × width (b) × height (d)), and each model is used for a different group of tests to study the effect of underground structure width on seepage characteristics.

Fine sand with a particle size less than 0.5 mm is used in the tests; the sand is sieved and layered into a model box after drying. The physical parameters are measured from the samples taken from the model box. The basic physical parameters of the sand are shown in Table 1.

2.3. Layout of the Monitoring Equipment. Figure 2 shows the layout of the water head monitoring tubes, which are thin-wall PVC pipes with a diameter of 20 mm, and are used to monitor the groundwater level at different burial depths, all of the pipe openings at the bottom of the monitoring tubes are covered with geotextiles to prevent sand particles from flowing into the tubes. There are 30 groundwater head monitors in total: they are arranged into three rows (A, B, and C), the spacing between each row is 200 mm, and the spacing between each measuring point in the same row is approximately 100 mm. The burial depths of the tubes in rows A, B, and C are 0.55 m, 0.45 m, and 0.4 m, respectively.

The pore water pressure sensors, which are arranged in a one-to-one correspondence with the position of the piezometer tubes, are used to measure the pore water pressure at the corresponding location. The measured data is collected by a DATATAKER data acquisition instrument.

2.4. Test Procedure. The test procedures are as follows:

2.4.1. Soil Filling and System Installation. Dry sand is poured into the box using a sand hopper, and the compaction of the sandy soil is carried out layer by layer with the thickness of the layer of 10 cm thick [36]. When the soil is filled to the

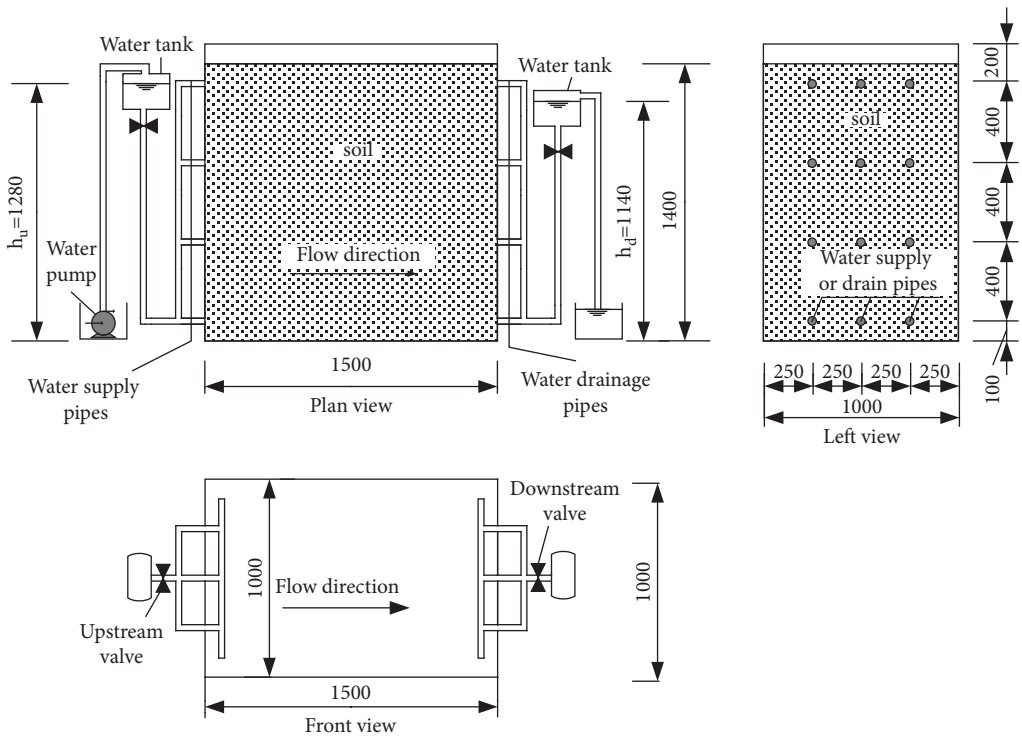

Figure 1: Schematic view of the laboratory test system (unit: mm).

Table 1: Parameters of the sand in laboratory test.

Parameter	Moisture density ρ (g·cm^{-3})	Dry density ρ (g·cm^{-3})	Pore ratio e	Hydraulic conductivity k (m·s^{-1})
Value	1.96	1.63	0.64	5.35×10^{-5}

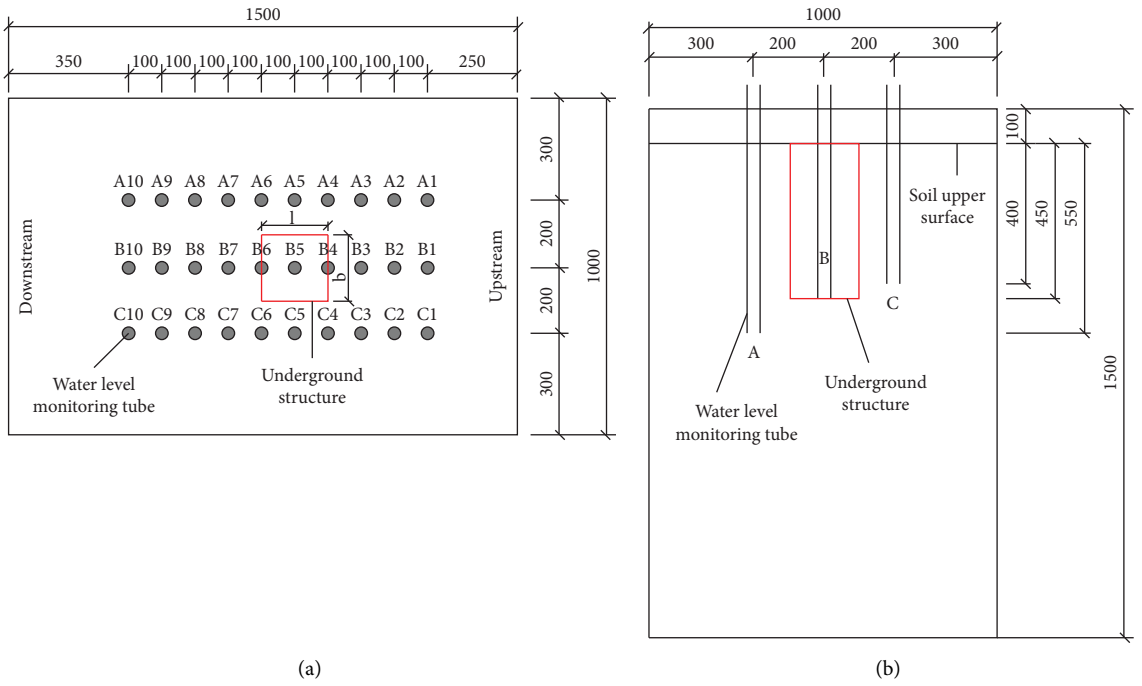

Figure 2: The layout of the water level monitoring tubes (unit: mm). (a) Plan view. (b) Vertical view.

height where the bottom of the structure and the water level monitoring tubes should be located, the structure model and the water level monitoring tubes are accurately positioned and installed, and their locations should be maintained until the filling reaches the predetermined height. Herein, the bottom of the structure is located at a depth of 0.45 m, and the bottoms of the water level monitoring tubes in rows A, B, and C are at depths of 0.55 m, 0.45 m, and 0.4 m, respectively, as shown in Figure 2.

2.4.2. Soaking and Saturation. After soil compaction, water is gradually poured into the tank through the upstream water supply pipes until the water level reaches the upper surface of the sand; careful attention is paid so that the sand was not disturbed. The water level is then kept at the same level as the upper surface of the sand for 24 h.

2.4.3. Seepage Test. During the seepage test, the water head is maintained at 1.28 m at the upstream boundary and at 1.14 m at the downstream boundary. The water supply and drainage pipes are kept open until the seepage is stable. The pore water pressure is monitored using pore water pressure sensors.

Four groups of tests with different structure widths were carried out via this procedure.

2.5. Test Results. Figure 3 shows the distribution of pore water pressure along the seepage direction at three different depths for different structure widths, where AP represents the calculation result according to Archimedes' principle. It can be seen that all the pore water pressure magnitude considering the groundwater seepage is generally greater than that calculated by Archimedes' principle, which shows that it is difficult to ensure the safety of a structure if the buoyancy is calculated via only Archimedes' principle.

Compared with the pore water pressure distribution in the absence of a structure, when an underground structure is present, a blocking effect on the groundwater seepage is expressed near the structure and the original seepage field is disturbed, which leads to a change in the pore water pressure distribution: an increase at the upstream side of the structure and a reduction at the downstream side. As the width b of the structure increases, the rate of increment/decrement gradually increases; furthermore, the closer to the structure, the greater increment/decrement is. Comparing the pore water pressure values at different depths in the three rows, it can be noticed that since the piezometer tubes in row A is located at the edge of the foundation and that the burial depth exceeds the bottom of the foundation, the presence of this underground structure has the least influence on the pore water pressure in row A; among the three rows, this underground structure has the greatest influence on the pore water pressure in row B since the piezometer tubes in that row are located on the centreline of the structure section and the burial depth is above the foundation bottom. Therefore, it can be concluded that the influence of the underground structure on the seepage is limited to the soil above the bottom of the foundation, affecting less in the soil below the bottom of the structure.

Figure 4 shows the distribution of the pore water pressure increment (an increment from that of no underground structure) at different locations at two sides of the underground structure. As the width of the structure increases, all of the pore water pressure gradually increases. The change at point B (at the centreline of the side of the structure) is the largest, followed by that at point C (the side edge of the structure), which is the smallest at point A (below the bottom). The pore water pressure at the structure side exhibits a "convex" distribution under different width conditions: the highest pressure occurs in the middle and the lowest pressure occurs on either side. Furthermore, the variation trends at the upstream and downstream sides are symmetrical.

3. Numerical Simulation of the Model Test

3.1. Finite Element Model. A 3D finite element model is established to simulate the physical model test. Figure 5 shows the FEM mesh of the 3D model, which is 1.5 m in length, 1.0 m in width, and 1.5 m in depth. In the FEM simulation, the soil is modeled using an eight-node hexahedron pore pressure element (C3D8P), and the parameter values are the same as those in the physical model test, as shown in Table 1. The underground structure is modeled by setting impermeable boundaries at the interfaces between the structure and the soil; the dimensions are the same as those used in the physical model tests. The boundary water level is consistent with that of the physical model test (i.e., 1.28 m at the upstream boundary and 1.14 m at the downstream boundary). A corresponding pore water pressure is applied at the boundary and is consistent with the hydrostatic pressure distributions at the upstream and downstream boundaries.

3.2. Comparison between the FEM and Physical Model Test Results. Figure 6 shows the pore water pressure results of the FEM analysis and the physical model test. The pore water pressure values at different locations of the physical model test are in good agreement with the corresponding FEM results, which indicates that the numerical simulation model is correct and can be accurately used for further discussion and analysis.

4. Parametric Study

The distribution of the groundwater level is a function of the hydraulic conductivity, seepage area, hydraulic gradient, and seepage time. The underground structure is a barrier to the recharge area, and the part that penetrates the aquifer is the barrier area. When the area of the structure increases, the seepage area decreases, and the flow rate and water level of the groundwater will change in the space and time domains [25]. This paper focuses on the situation in which seepage is stable. Therefore, the structural dimension (seepage area), hydraulic gradient, and hydraulic conductivity ratio k_1/k_2

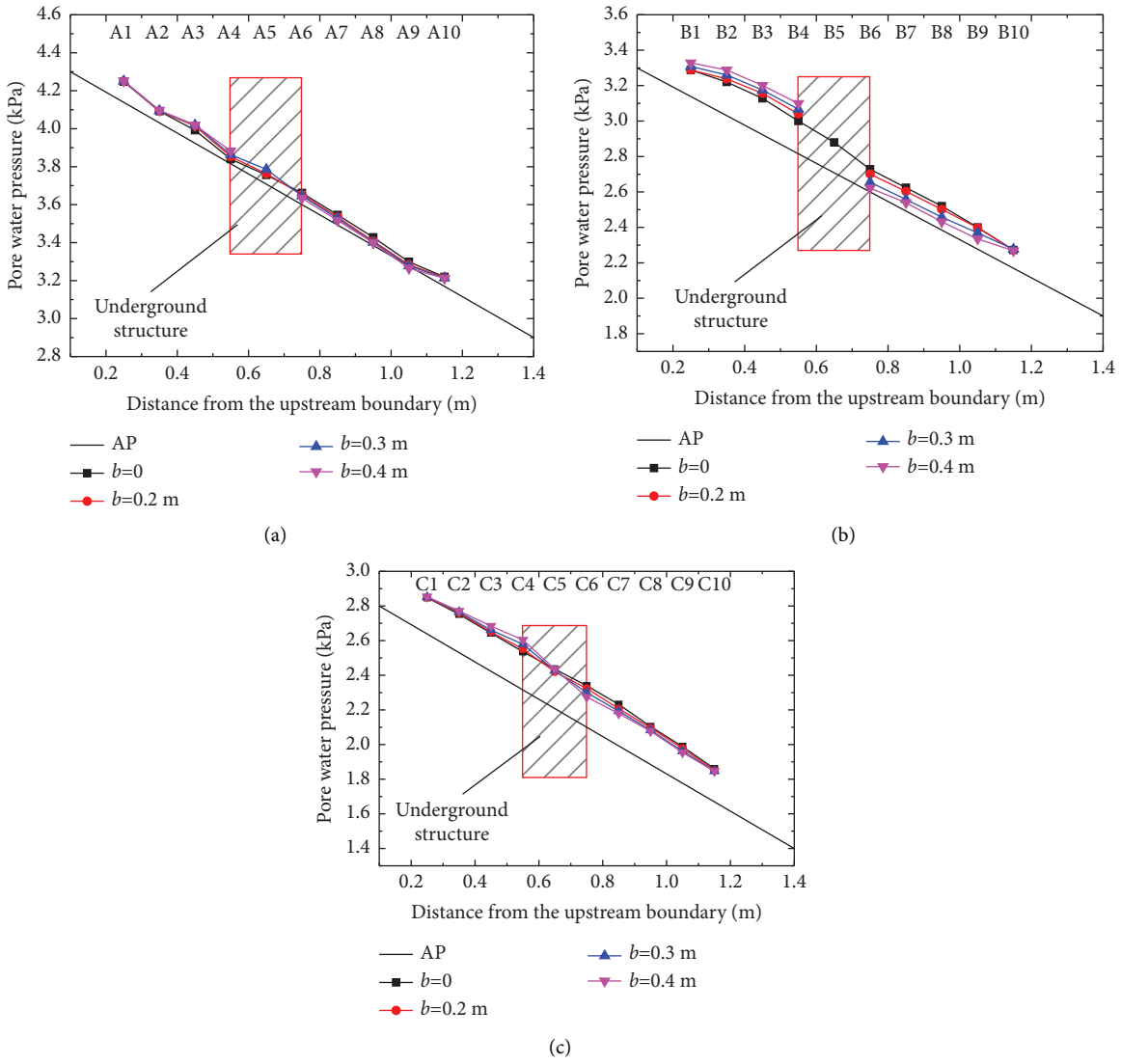

Figure 3: Longitudinal distribution of pore water pressure for different structure widths. (a) Row A. (b) Row B. (c) Row C.

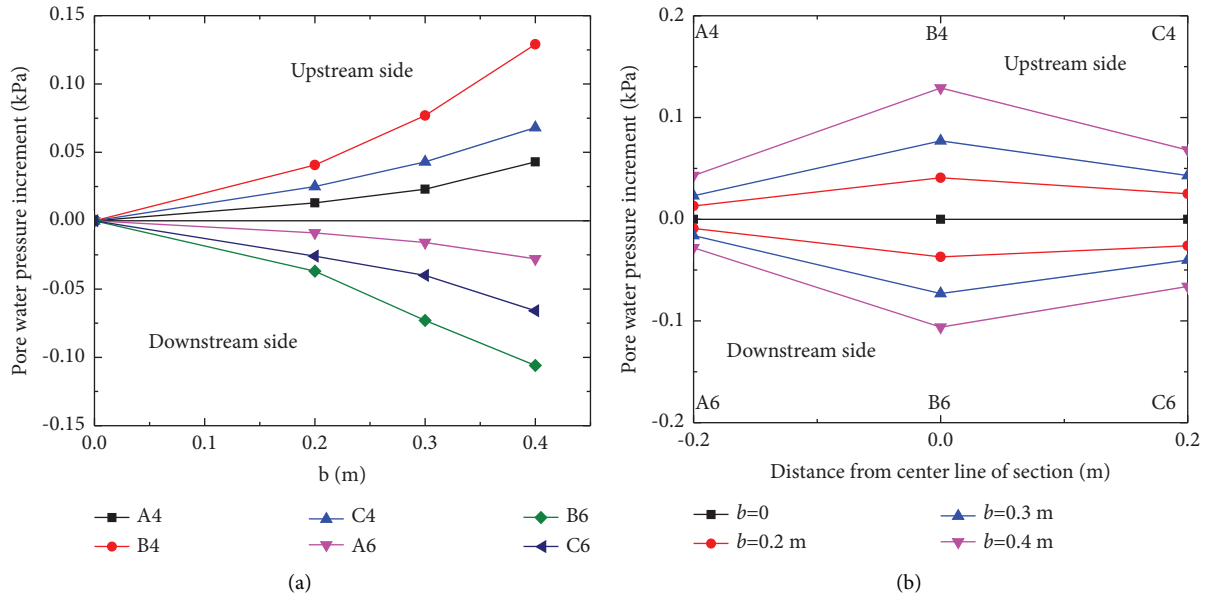

Figure 4: Variation in the pore water pressure increment at two sides of the structure. (a) Variation in pore water pressure increment with the width of the structure. (b) Distribution of pore pressure at both sides of the structure.

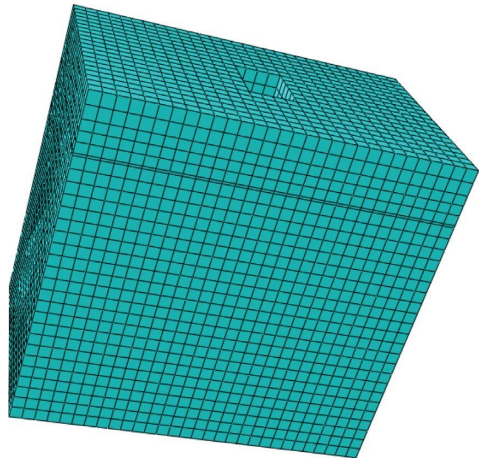

Figure 5: Schematic of the finite element mesh.

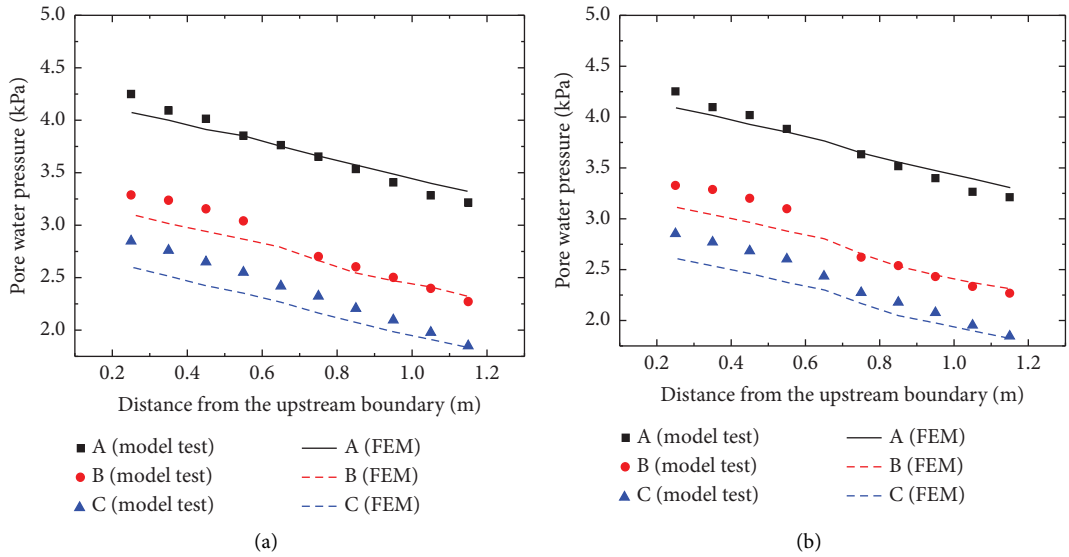

Figure 6: Comparison of the pore water pressures from the FEM and physical model test results. (a) $b = 0.2$ m. (b) $b = 0.4$ m.

between different layers in two-layer soil are selected for research.

4.1. Boundary Effect. When the groundwater seepage is numerically simulated, some impervious boundaries should be set, which will affect the results of the seepage field; this is called a boundary effect. However, in actual engineering, impervious boundaries are rare, or such boundaries are far from the underground structure and thus can be ignored. Therefore, the boundary effect must be determined before the parametric study, and reasonable relative dimensions of the model can be determined.

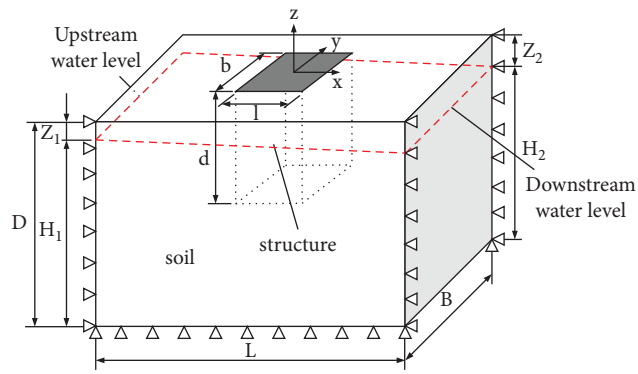

Figure 7: Schematic of the seepage model.

4.1.1. FEM Model. A schematic diagram of the seepage model is shown in Figure 7. The soil is homogeneous, and the soil parameter values are the same as those shown in Table 1. The structure width is $b = 40$ m, the length is $l = 10$ m, and the insertion depth is $d = 30$ m. The deformation of the model is restricted throughout the seepage process to ensure that the dimensions of the underground structure remain constant and the hydraulic gradient is maintained at 2%. Then, the boundary effect is

studied by changing the width, length, and height of the whole mesh.

4.1.2. Results. Figure 8 shows a schematic of the underground water level distribution, where line *a*–*d* represents the original water level (no underground structure), lines *a*–*e* and *f*–*d* represent the actual water level, and lines *a*-*b* and *c*-*d* are the calculation baselines, which are selected at the corresponding heights of the upstream and downstream boundary water levels (H_1, H_2). Since the pore water pressure is approximately linearly distributed along the vertical direction, the Lagrange linear interpolation method can be used to calculate the water level height as follows:

$$h_{zx} = \frac{P_{zx} - P_{1x}}{P_{2x} - P_{1x}} \left(H_2 - H_2\right) + H_{1,} \tag{1}$$

where h_{zx} and P_{zx} are the groundwater level and the corresponding pore water pressure, $P_{zx} = 0$. H_1 and H_2 are the heights at the selected baselines, and P_{1x} and P_{2x} are the pore water pressures calculated with the FEM at the baselines.

To better illustrate the seepage field distribution change in the following discussion, this is best shown in a dimensionless form using the maximum water level increment ratio (MWLIR) η, which is defined as follows:

$$\eta = \frac{\left(h_b - h_0\right)}{il}, \tag{2}$$

where h_b is the maximum water level at the side of the underground structure when the structure width is b, h_0 is the original water level, then $(h_b - h_0)$ is the maximum water level increment (MWLI). i is the hydraulic gradient, l is the structure length, then il is the water level reduction within length l when there is no structure, as shown in Figure 8.

Since the distributions at two sides of the structure are symmetrical to each other, only the upstream side is selected for analysis ($x = -l/2$). In the following discussion, $x = -l/2$ represents the upstream side, and $x = l/2$ represents the downstream side. Figure 9 shows the variation in MWLIR when the model dimensions ratio changes. Obviously, the MWLIR is only slightly influenced by the dimension ratio when the width ratio of the underground structure to model (b/B) is less than 0.4, the length ratio (l/L) is less than 0.1, and the depth ratio (d/D) is less than 0.6. Then it can be concluded that the seepage field distribution is not affected by the boundary effect when the above-mentioned dimensional requirements are satisfied. Therefore, this scheme is used as the basis for the relative dimension determination of the subsequent FEM.

4.2. Influence of the Underground Structure Dimensions. The whole mesh dimension is set as 200 m × 200 m × 100 m (length × width × height); considering the influence of the boundary effect, the investigated widths of the underground structure are 0 m, 10 m, 20 m, and 40 m; the lengths are 0 m, 10 m, 20 m, and 40 m; and the insertion depths are 0 m, 15 m, 30 m, and 60 m. The soil is homogeneous, and the soil parameters are the same as those shown in Table 1; the hydraulic gradient is 2%.

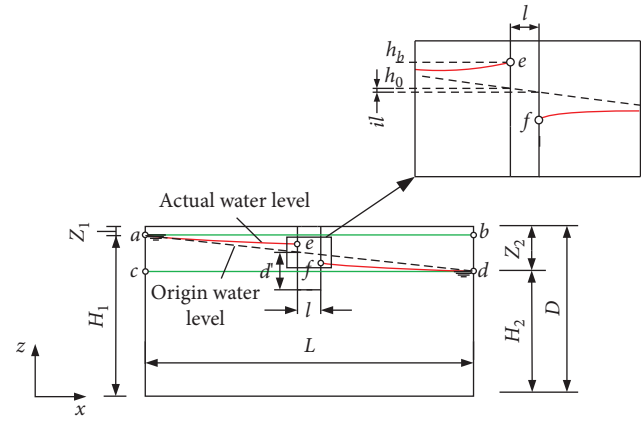

Figure 8: Schematic of underground water level distribution.

Figure 10 shows the variation in MWLI ($h_b - h_0$) at the side of the structure as the structure dimension changes. As the structure dimension (length, width, or insertion depth) increases, the water level gradually increases as well, but the influence degrees are different. Among them, the width change has a significant effect on the groundwater level. Although there is a slight impact on the groundwater level when the structure length is short, when the length is greater than 30 m, the influence can be ignored. Similarly, the insertion depth effect is limited to conditions with a structure depth shallower than 30 m. When the depth is deeper than 30 m, there is no insertion depth effect. According to the test results presented in this section, of the three dimensions, the structure width has the largest effect, followed by the insertion depth, and the length has the smallest effect on the MWLI.

4.3. Influence of the Hydraulic Gradient. In the following work, the hydraulic gradient is set to 1%, 2%, and 4%. Since the structure length has little influence on MWLI, the structure length is set to 10 m and remains unchanged in the following discussion. The insertion depth is 30 m, and the structure width is set to 10 m, 20 m, and 40 m. The soil parameters are the same as those shown in Table 1.

Figure 11 shows the variation in MWLI at the structure side when the hydraulic gradient changes. The MWLI increases with the increase in the hydraulic gradient under different structure widths, this is consistent with the statement in [22], and the rate of increase is related to the width; the larger the structure width, the faster the increase in the MWLI. Furthermore, the water level changes at two sides of the structure are symmetrical. Although the MWLI is influenced by the hydraulic gradient, the MWLIR is constant under a certain width and does not change with the change in hydraulic gradient because of the linear relationship between the maximum water level increment ($h_b - h_0$) and head reduction value il for a certain width.

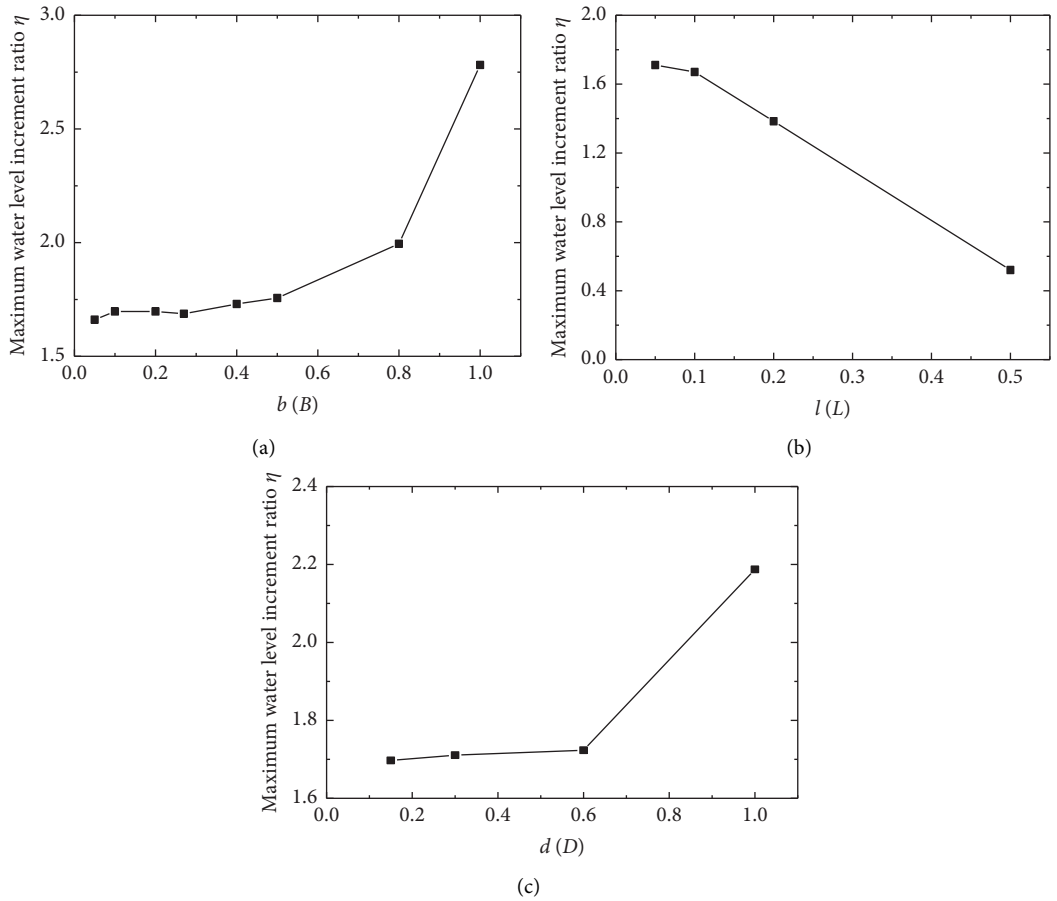

Figure 9: Variation in MWLIR with model relative dimension. (a) Influence of width ratio b/B. (b) Influence of length ratio l/L. (c) Influence of height ratio d/D.

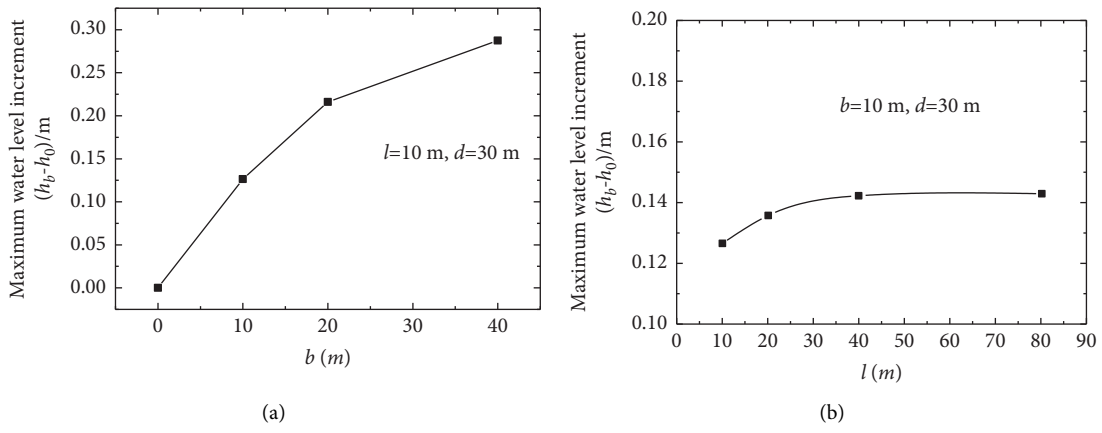

Figure 10: Continued.

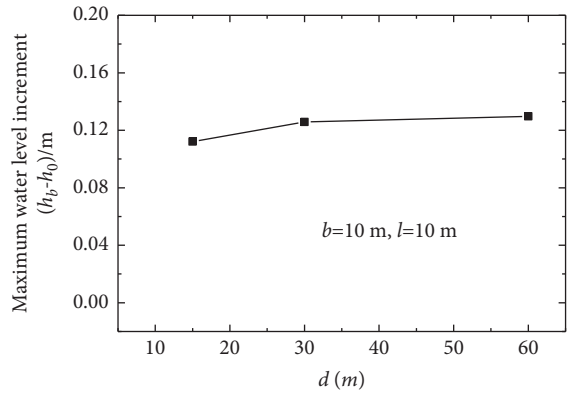

(c)

Figure 10: Variation in MWLIR with structure dimensions (a) Influence of the structure width b. (b) Influence of the structure length l. (c) Influence of the structure insertion depth d.

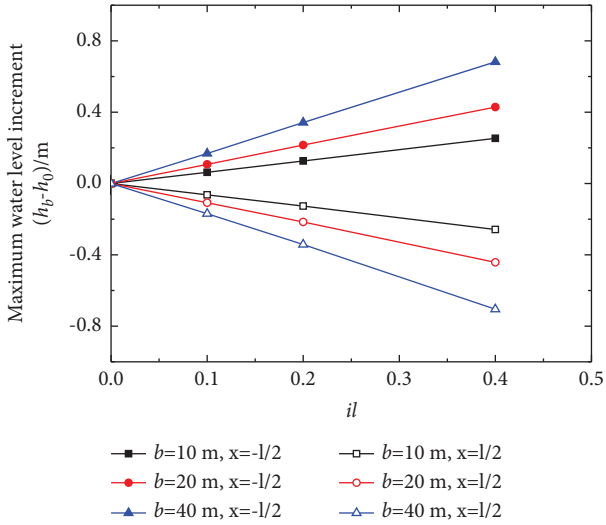

Figure 11: Variation in MWLI with the hydraulic gradient.

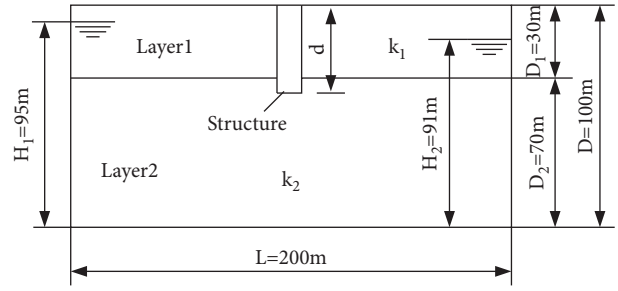

Figure 12: Schematic view of the two-layer soil.

4.4. The Hydraulic Conductivity Ratio k_1/k_2. Figure 12 shows a two-layer soil system. The hydraulic conductivity ratios between the two layers (k_1/k_2) are set as 10^{-4}, 10^{-3}, 10^{-2}, 0.5, 0.1, and 1 (working conditions GK1 to GK6), and the hydraulic conductivity of the lower layer k_2 is set to 1×10^{-3} m/s. The structure width is set to 10 m, 20 m, and 40 m, and the length is 10 m; considering different depths of the structure inserted into the lower soil, the insertion depth of the structure is set to 30 m, 40 m, 50 m, and 60 m. Partial calculation results are shown in Table 2.

The results show that the difference between the soil hydraulic conductivity of different soil layers has a certain influence on the groundwater level change for the same underground structure. Specifically, the greater the hydraulic conductivity of the upper soil, the greater the water level increment. The phenomenon can be attributed to that: while the structure dimensions remain constant, the seepage lengths are similar as well for a different condition, then from the Darcy's Law [37], the head loss in one soil layer is inversely proportional to the hydraulic conductivity of the soil, that is, the greater hydraulic conductivity, the less head loss in the soil, then the water level at the structure side is relatively higher.

5. Simplified Groundwater Level Calculation Method

5.1. Homogeneous Soil. From the analysis performed, the water level distribution at the structure side has a convex shape. Defining the water level difference ratio (WLDR) ξ as follows:

$$\xi = \frac{h_y - h_{y=100}}{h_{y=0} - h_{y=100}}, \tag{3}$$

where h_y is the water level height at the location with the lateral coordinate y, e.g., $h_{y=100}$ is the water level height when the lateral coordinate y is 100. When the distance from the structure is far, the water level change is only slightly affected by the structure, and the water level is almost equal to that when there is no structure h_0. $h_{y=0}$ is the water level at the centreline of the side of the structure and is the maximum water level over the entire section h_b. Then, the difference between the two ($h_{y=0} - h_{y=100}$) is the maximum water level increment at the side of the structure compared with the condition of no structure, which is equal to ($h_b - h_0$) above.

Table 2: Comparison of water level increment ratios caused by a hydraulic conductivity ratio change.

b (m) × l (m) × d (m)	$\Delta h_i - \Delta h_1/il$					
	GK1	GK2	GK3 (%)	GK4 (%)	GK5 (%)	GK6 (%)
40 × 10 × 40	0	0	0.2	0.9	1.7	10.5
40 × 10 × 50	0	0	0.1	0.6	1.1	6.5

Note. Δh_i is the maximum water level increment corresponding to the working condition $GK_i\,(i = 1, 2, \cdots 6)$.

Figure 13 shows the lateral distribution curve of the WLDR at the side of the structure in homogeneous soil. This result approximately obeys a normal distribution and has a certain relationship with the width of the structure, while the depth has little influence on the distribution. Then, curve fitting was performed, and empirical estimation of WLDR at the upstream side was obtained by the following formula, due to the symmetry at two sides of the structure, the corresponding results at the downstream side can be obtained by adding a minus sign to the right of the following formula, and the later formulas are only for the upstream as well, the results at the downstream can be obtained by the same procedure.

$$\frac{h_y - h_{y=100}}{h_{y=0} - h_{y=100}} = \frac{h_y - h_0}{h_b - h_0} = e^{-\left[1.03+0.6e^{-0.05b}\right](2y/b)^2}\left(x = \frac{-l}{2}, -\frac{b}{2} \le y \le \frac{b}{2}\right). \tag{4}$$

The MWLI $(h_b - h_0)$ is required to calculate the distribution of the water level. However, it is related to the width and insertion depth of the structure from the analysis performed.

Figure 14 shows the variation in the MWLIR, η, with the effective depth-width ratio (d'/b) of the structure. This method of presenting the results is adopted because it is more general and enables simple allowance for the effect of differences in geometry. It can be noticed that the MWLIR decreases with the increase in the effective depth-width ratio, and the upstream and downstream variation trends are symmetrical to each other. For he homogeneous soil, the MWLIR can be obtained by the following formula when the seepage is steady.

$$\eta = \frac{h_b - h_0}{i \cdot l} = 0.24\left(\frac{d'}{l}\right) \cdot \ln\left(\frac{d'}{b}\right) - \frac{0.47d'}{l}\left(x = \frac{-l}{2}\right), \tag{5}$$

where d' is the effective depth of the structure, which is defined as the maximum depth below the groundwater level without an underground structure, as shown in Figure 8. This result arises because the groundwater level varies depending on the in situ conditions; thus, it is more reasonable to express the depth via the effective depth.

Consequently, the MWLI can be given by the following normalization form:

$$h_b - h_0 = i \cdot \left[0.24d' \cdot \ln\left(\frac{d'}{b}\right) - \frac{0.47d'}{l}\right]\left(x = \frac{-l}{2}\right). \tag{6}$$

Then, by substituting the formulas (6) into formula (4), the water level h_y at any position along the structure side in the homogeneous soil can be obtained.

5.2. Two-Layer Soil. Figure 15 shows the lateral distribution curve of the WLDR at the side of the structure in two-layer soil for different hydraulic conductivity ratios. It is shown that the variation in the hydraulic conductivity ratio does not affect the lateral distribution of the WLDR. That is, the WLDR of two-layer soil can be calculated by the formula (4) for homogeneous soil.

Although the variation in the hydraulic conductivity ratio does not affect the lateral distribution of the WLDR, from the analysis in Section 4.4, the MWLIR in the two-layer soil is related to the hydraulic conductivity ratio, which is required to obtain the water level height h_y. Figure 16 shows the variation in the MWLIR with the effective depth-width ratio of the structure under different hydraulic conductivity ratios. It can be seen that the hydraulic conductivity ratio has a certain influence on the MWLIR. The MWLIR decreases with the increase in the effective depth-width ratio and the variation trends for different hydraulic conductivity ratios are similar. Then, curve fitting can be performed to obtain the MWLIR, which can be expressed as follows:

$$\frac{(h_{bk} - h_0)}{(i \cdot l)} = A \ln\left(\frac{d'}{b}\right) + B, \tag{7}$$

where h_{bk} is the maximum water level height at the side of the underground structure under different hydraulic conductivity ratio in two-layer soil, and A and B are the fitting parameters related to the soil hydraulic conductivity.

To extend the above results to an arbitrarily two-layer soil, a simplified method for the soil layer is proposed. An arbitrary two-layer soil, as shown in Figure 12, can be simplified into two layers bounded by the bottom of the structure through the equivalent hydraulic conductivity method, as shown in Figure 17. The equivalent hydraulic conductivity of the upper soil layer can be calculated by the following formula, while the hydraulic conductivity of the lower soil layer remains k_2.

$$k_1' = \frac{[k_1 D_1 + k_2 (d - D_1)]}{d}. \tag{8}$$

The simplified two-layer soil is used for numerical simulation to check the correctness of the soil layer simplification method. Table 3 shows the comparison of the MWLI value obtained by the simulation between the actual soil layer and the simplified soil layer; the results are very similar, so the method is considered to be effective.

The change law of coefficients A and B in formula (7) with the equivalent hydraulic conductivity ratio k_1'/k_2 is shown in Figure 18. The MWLIR can be obtained by the following formula:

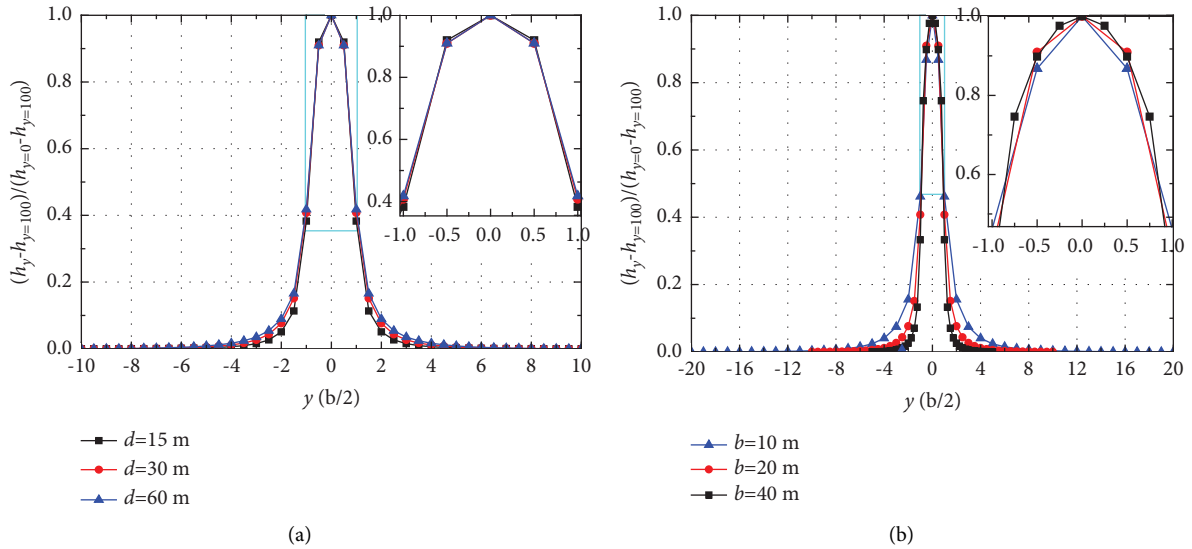

Figure 13: Lateral distribution of the WLDR at the side of the structure in homogeneous soil. (a) $b = 20$ m, $l = 10$ m. (b) $d = 30$ m, $l = 10$ m.

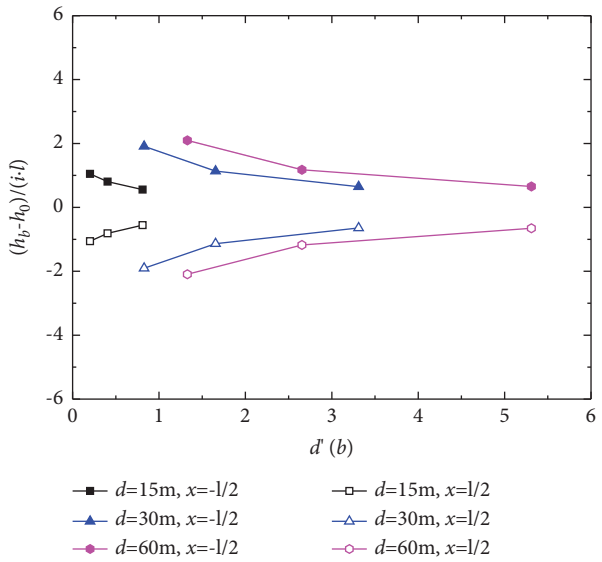

Figure 14: Variation in the MWLIR with the effective depth-width ratio of the structure.

$$\eta = \frac{h_{bk} - h_0}{il} = \left[-0.025 \cdot \ln\left(\frac{k_1'}{k_2}\right) + 0.24\right] \cdot \frac{d'}{l} \cdot \ln\left(\frac{d'}{b}\right) + \frac{d'}{l} \cdot \left[-0.03 \cdot \ln\left(\frac{k_1'}{k_2}\right) - 0.47\right] \left(x = \frac{-l}{2}\right). \tag{9}$$

Consequently, the MWLI in the two-layer soil at the structure side can be given by the following form:

$$h_{bk} - h_0 = i \cdot \left\{\left[-0.025 \cdot \ln\left(\frac{k_1'}{k_2}\right) + 0.24\right] \cdot d' \cdot \ln\left(\frac{d'}{b}\right) + d' \cdot \left[-0.03 \cdot \ln\left(\frac{k_1'}{k_2}\right) - 0.47\right]\right\} \left(x = \frac{-l}{2}\right). \tag{10}$$

Similarly, substituting formulas (10) into (4), the water level in two-layer soil at any location along the structure side h_y' can be obtained.

Since the soil layers in the field are generally comprised of several layers, rather than the simply two-layer above, therefore, further soil equivalence need should be carried

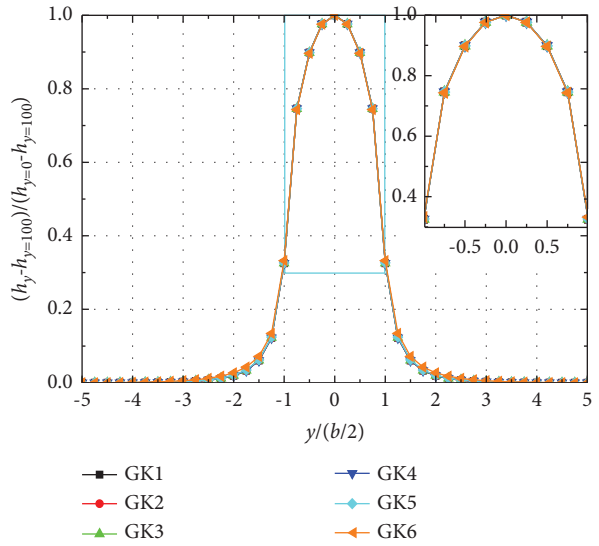

Figure 15: Lateral distribution of the WLDR at the side of the structure in two-layer soil ($b = 40$ m, $l = 10$ m, $d = 30$ m).

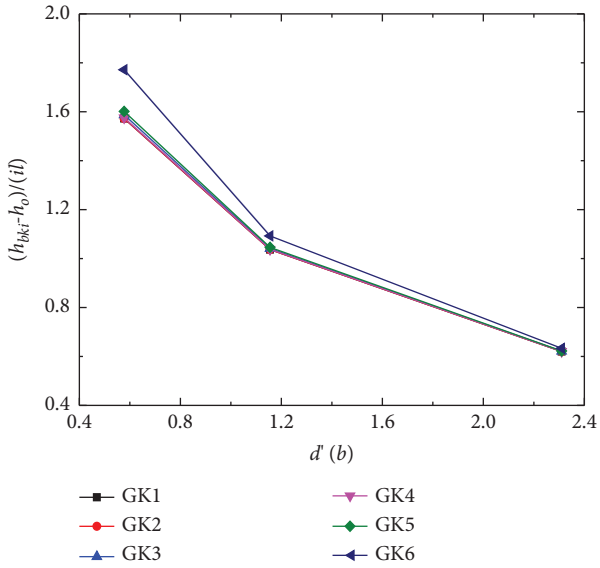

Figure 16: Variation in the MWLIR with the effective depth-width ratio of the structure in a two-layer soil ($d = 30$ m, $x = -l/2$).

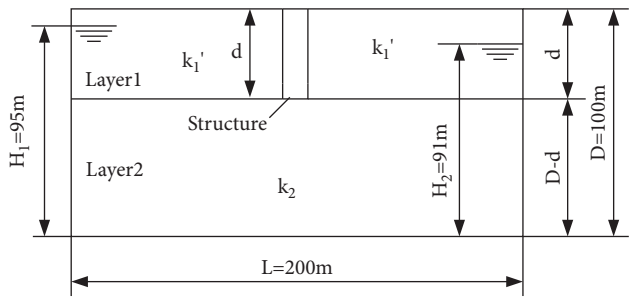

Figure 17: Simplified schematic diagram of two-layer soil.

Table 3: Comparison of the MWLIs obtained by simulation considering the actual soil layer and the simplified soil layer.

Work condition	$b \times l \times d$	MWLI (m)	
		Actual soil layer	Simplified soil layer
GK1	40 m × 10 m × 40 m	−0.354	−0.361
GK1	10 m × 10 m × 40 m	−0.128	−0.128

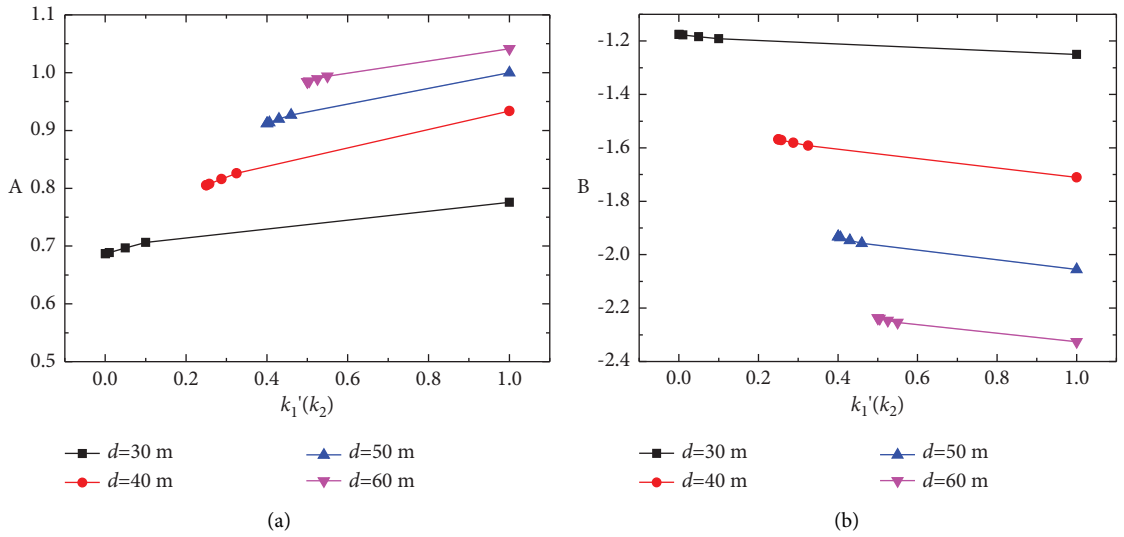

Figure 18: Variation in the coefficients for different equivalent hydraulic conductivity ratios. (a) Coefficient A. (b) Coefficient B.

out. For an arbitrary multilayer soil, as shown in Figure 19, it can also be simplified into a two-layer soil model bounded by the structure bottom. The corresponding equivalent hydraulic conductivity can be calculated as follows [37]:

$$k_1' = \frac{\sum_{i=1}^{n} k_{ui} \cdot d_{ui}}{d}, \tag{11a}$$

$$k_2' = \frac{\sum_{j=1}^{m} k_{dj} \cdot d_{dj}}{D - d}, \tag{11b}$$

where k_{ui} and d_{ui} are the hydraulic conductivity and the thickness of the i-th layer above the structure baseplate, k_{dj} and d_{dj} are those in the j-th layer below the structure baseplate. Then, substituting these two expressions into formula (10), k_2 in formula (10) equals k_2', then the maximum water level increment can be obtained.

6. Verification of the Simplified Method

Figure 20 shows a three-layer soil system, the top layer has a thickness (D_1) of 30 m and a hydraulic conductivity (k_1) of 5×10^{-6} m/s, while those in the intermediate layer are 30 m and 1×10^{-4}m/s (D_2, k_2), and those in the bottom layer are 40 m and 1×10^{-5} (D_3, k_3). The structure length is 10 m, it penetrates the intermediate layer, and the insertion depth is 40 m. Then, the equivalent hydraulic conductivity k_1' and k_2' are 2.87×10^{-5}m/s and 4×10^{-5}m/s, respectively, the hydraulic conductivity ratio is 0.72. Table 4 shows the comparison of the MWLI results obtained by the numerical simulation and the simplified calculation method. The results from the simplified method are larger, but the errors are relatively small, and the simplified calculation method is considered to be effective.

7. Discussion

The results of this study indicate that the magnitude of groundwater level variation depends on the location of the points across the underground structure, the maximum head rise (or drop) commonly occurs close to the barrier and diminishes as the distance is increased, which is consistent with the previous study [20]. Unlike in which the calculation method for the maximum head rise is only provided, this study stresses that the nonuniform distribution ("convex" distribution) also exhibits at the structure sections, which can be explained by the bypass effect that the dimension of the structure perpendicular to seepage direction in engineering practice is always limited. It is further explained it would overestimate the effect based on the 2D or quasi-2D problem. Furthermore, although the researched parameters affect the maximum head rise significantly, there is little difference in the distribution form at the structure section for different parameters. That is very useful in predicting the groundwater level with different effect factors. The proposed empirical formulas make a further contribution to the calculation of the groundwater level around the structure and provide the basis for the prediction of the groundwater level to make a more reasonable antifloating design for the underground structure. However, the soil layer simplification method adopted in the study is limited to the head

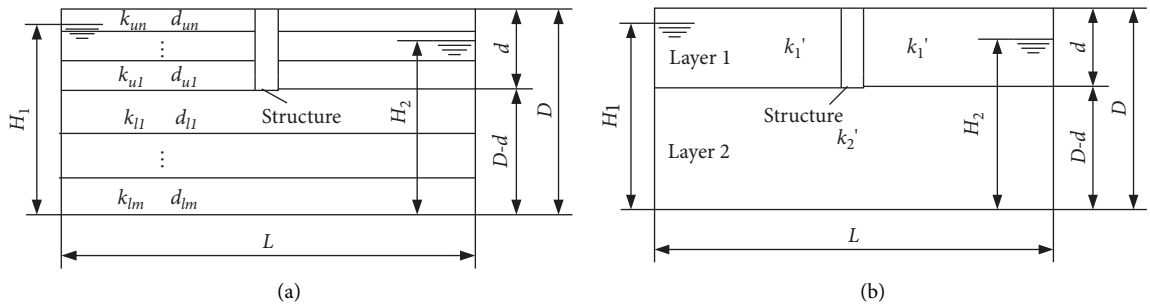

Figure 19: Multilayer soil simplification schematic diagram. (a) Multilayer soil diagram. (b) Simplified two-layer soil.

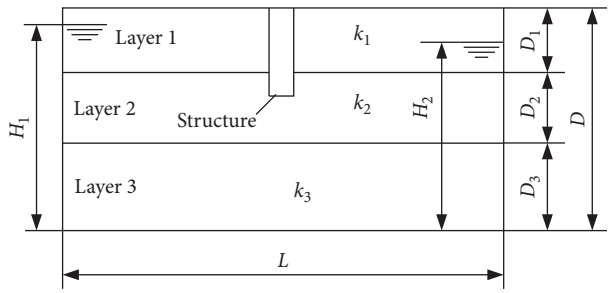

Figure 20: Three-layer soil distribution and equivalent diagram.

Table 4: Comparison of the MWLI obtained by the simulation and the simplified calculation method6t.

Dimensions b (m) × l (m) × d (m)	MWLI (m)		Error (%)
	FEM	Simplified methods	
10 × 10 × 40	−0.128	−0.108	15
20 × 10 × 40	−0.237	−0.224	5.5
40 × 10 × 40	−0.355	−0.335	5.6

difference between the upstream boundary and the downstream boundary, in engineering practice, it depends on the regional hydraulic gradient, the greater gradient, the larger error would occur by using this simplification method. Extension of the present work may consist in considering a more appropriate equivalent method to simplify the multilayer soil; furthermore, the aquifer thickness is not considered in the paper, which would affect the mechanism of the water level variation, for example, in the case that an underground structure completely reduces the aquifer section along the vertical direction totally.

8. Conclusions

Through physical model testing and numerical analysis, the distribution of groundwater seepage in the presence of underground structures under different influencing factors were studied. On this basis, the hydrostatic head near the underground structure was corrected. The conclusions are as follows:

(1) The underground structure has a barrier effect on the groundwater seepage: the water level rises on the upstream side and decreases on the downstream side. As the width of the underground structure increases, the water level increases, but the influence is limited to the soil above the bottom of the foundation, which is less in the soil present below the foundation. The pore water pressure exhibits a roughly "convex" distribution at the side of the structure.

(2) In homogeneous soil, the width of the structure has the greatest influence on the seepage field, followed by the insertion depth, and the length has the least influence. The hydraulic gradient has a significant effect on the water level increment but does not affect the MWLIR. In multilayer soil, the hydraulic conductivity ratio between different soil layers affects the distribution of the groundwater level.

(3) Based on the numerical simulation results, a simplified formula for calculating the water level distribution at the side of the underground structure under different working conditions is obtained. Further extension is developed to apply the formula in multilayer soil through an equivalent hydraulic conductivity method, and the effectiveness of the simplified method is verified by some examples.

Data Availability

All the data are included in the manuscript from the corresponding author upon request.

Conflicts of Interest

The authors declare that they have no conflicts of interest.

Acknowledgments

The author would like to acknowledge the support from the Shaanxi Key Laboratory for the Property and Treatment of Special Soil and Rock (KF2020-06), Shaanxi Province Key R&D Program (2020ZDLSF06-03), CMEC 2017 Science and Technology R&D Fund Project (CMECKJYF-2017-05), and the Shanghai Natural Science Foundation (22ZR1464600).

References

[1] S. M. Liao, S. F. Wei, and S. L. Shen, "Structural responses of existing metro stations to adjacent deep excavations in suzhou, China," *Journal of Performance of Constructed Facilities*, vol. 30, no. 4, Article ID 04015089, 2016.

[2] X. X. Liu, S. L. Shen, A. Zhou, and Y. S. Xu, "Evaluation of foam conditioning effect on groundwater inflow at tunnel cutting face," *International Journal for Numerical and Analytical Methods in Geomechanics*, vol. 43, no. 2, pp. 463–481, 2019.

[3] J. Zhang, S. Lu, T. Feng, B. Yi, and J. Liu, "Research on reuse of silty fine sand in backfill grouting material and optimization of backfill grouting material proportions," *Tunnelling and Underground Space Technology*, vol. 130, Article ID 104751, 2022.

[4] F. L. Peng, H. L. Wang, Y. Tan, Z. L. Xu, and Y. L. Li, "Field measurements and finite-element method simulation of a tunnel shaft constructed by pneumatic caisson method in Shanghai soft ground," *Journal of Geotechnical and Geoenvironmental Engineering*, vol. 137, no. 5, pp. 516–524, 2011.

[5] J. J. Chen, L. Y. Zhang, J. F. Zhang, Y. F. Zhu, and J. H. Wang, "Field tests, modification, and application of deep soil mixing method in soft clay," *Journal of Geotechnical and Geoenvironmental Engineering*, vol. 139, no. 1, pp. 24–34, 2013.

[6] J. Zhang, Y. Liang, and T. Feng, "Investigation of the cause of shield-driven tunnel instability in soil with A soft upper layer and hard lower layer," *Engineering Failure Analysis*, vol. 118, Article ID 104832, 2020.

[7] O. P. M. Vitali, T. B. Celestino, and A. Bobet, "Buoyancy effect on shallow tunnels," *International Journal of Rock Mechanics and Mining Sciences*, vol. 114, pp. 1–6, 2019.

[8] J. W. Zhang, J. Cao, L. Mu, L. Wang, and J. Li, "Buoyancy Force Acting on Underground Structures Considering Seepage of Confined Water," *Complexity*, vol. 2019, Article ID 7672930, 2019.

[9] Q. Zhang, L. Ouyang, Z. Wang, H. Liu, and Y. Zhang, "Buoyancy reduction coefficients for underground silos in sand and clay," *Indian Geotechnical Journal*, vol. 49, no. 2, pp. 216–223, 2019.

[10] L. Song, X. Kang, and G. Mei, "Buoyancy force on shallow foundations in clayey soil: an experimental investigation based on the "Half Interval Search"," *Ocean Engineering*, vol. 129, pp. 637–641, 2017.

[11] Y. S. Xu, L. Ma, S. L. Shen, and W. J. Sun, "Evaluation of land subsidence by considering underground structures that penetrate the aquifers of Shanghai, China," *Hydrogeology Journal*, vol. 20, no. 8, pp. 1623–1634, 2012.

[12] Y. X. Wu, S. L. Shen, and D. J. Yuan, "Characteristics of dewatering induced drawdown curve under blocking effect of retaining wall in aquifer," *Journal of Hydrology*, vol. 539, pp. 554–566, 2016.

[13] C. F. Zeng, H. Liao, X. L. Xue et al., "Responses of groundwater and soil to dewatering considering the barrier effect of adjacent metro station on multi-aquifers," *Journal of Hydrology*, vol. 612, Article ID 128117, 2022.

[14] J. Wang, X. Liu, S. Liu, Y. Zhu, W. Pan, and J. Zhou, "Physical model test of transparent soil on coupling effect of cut-off wall and pumping wells during foundation pit dewatering," *Acta Geotechnica*, vol. 14, no. 1, pp. 141–162, 2018.

[15] X. W. Wang, T. L. Yang, Y. S. Xu, and S. L. Shen, "Evaluation of optimized depth of waterproof curtain to mitigate negative impacts during dewatering," *Journal of Hydrology*, vol. 577, Article ID 123969, 2019.

[16] Y. X. Wu, S. L. Shen, H. M. Lyu, and A. Zhou, "Analyses of leakage effect of waterproof curtain during excavation dewatering," *Journal of Hydrology*, vol. 583, Article ID 124582, 2020.

[17] Y. S. Xu, X. X. Yan, S. L. Shen, and A. N. Zhou, "Experimental investigation on the blocking of groundwater seepage from a waterproof curtain during pumped dewatering in an excavation," *Hydrogeology Journal*, vol. 27, no. 7, pp. 2659–2672, 2019.

[18] G. Ding, J. J. Jiao, and D. Zhang, "Modelling study on the impact of deep building foundations on the groundwater system," *Hydrological Processes*, vol. 22, no. 12, pp. 1857–1865, 2008.

[19] G. Ricci, R. Enrione, A. Eusebio, and R. Crova, "Numerical modelling of the interference between underground structures and aquifers in urban environment," in *The Turin subway – line 1 Underground Space*, H. Barták and Z. Romancov, Eds., pp. 1323–1329, Taylor and Francis Group, London, UK, 2007.

[20] E. Pujades, A. López, J. Carrera, E. Vázquez-Suñé, and A. Jurado, "Barrier effect of underground structures on aquifers," *Engineering Geology*, vol. 145-146, pp. 41–49, 2012.

[21] M. Deveughèle, P. Zokimila, and R. Cojean, "Impact d'une galerie étanche peu profonde sur l'écoulement d'une nappe," *Bulletin of Engineering Geology and the Environment*, vol. 69, no. 1, pp. 143–152, 2009.

[22] J. Font-Capo, E. Pujades, E. Vàzquez-Suñé, J. Carrera, V. Velasco, and D. Montfort, "Assessment of the barrier effect caused by underground constructions on porous aquifers with low hydraulic gradient: a case study of the metro construction in Barcelona, Spain," *Engineering Geology*, vol. 196, pp. 238–250, 2015.

[23] J. J. Jiao, X. S. Wang, and S. Nandy, "Preliminary assessment of the impacts of deep foundations and land reclamation on groundwater flow in a coastal area in Hong Kong, China," *Hydrogeology Journal*, vol. 14, no. 1-2, pp. 100–114, 2004.

[24] P. Marinos and M. Kavvadas, "Rise of the groundwater table when flow is obstructed by shallow tunnels," in *Proceedings of the Groundwater in the Urban Area: Problems Processes and Management. 27th Cong*, pp. 21–27, International Association Hydrogeologists (IAH), Nottingham, UK, 1997.

[25] Y. S. Xu, *Evaluation of the Behavior of Groundwater Seepage and Land Subsidence via Considering Infrastructures Inserted*

in aquifers(PhD Thesis), Shanghai Jiao Tong University, Shanghai, China, 2010.

[26] Y. S. Xu, S. L. Shen, Y. J. Du, J. C. Chai, and S. Horpibulsuk, "Modelling the cutoff behavior of underground structure in multi-aquifer-aquitard groundwater system," *Natural Hazards*, vol. 66, no. 2, pp. 731–748, 2012b.

[27] Y. S. Xu, S. L. Shen, L. Ma, W. J. Sun, and Z. Y. Yin, "Evaluation of the blocking effect of retaining walls on groundwater seepage in aquifers with different insertion depths," *Engineering Geology*, vol. 183, pp. 254–264, 2014.

[28] Y. Yihdego, "Evaluation of flow reduction due to hydraulic barrier engineering structure: case of urban area flood, contamination and pollution risk assessment," *Geotechnical & Geological Engineering*, vol. 34, no. 5, pp. 1643–1654, 2016.

[29] S. L. Shen, Y. X. Wu, and A. Misra, "Calculation of head difference at two sides of a cut-off barrier during excavation dewatering," *Computers and Geotechnics*, vol. 91, pp. 192–202, 2017.

[30] X. W. Wang and Y. S. Xu, "Impact of the depth of diaphragm wall on the groundwater drawdown during foundation dewatering considering anisotropic permeability of aquifer," *Water*, vol. 13, no. 4, p. 418, 2021.

[31] M. A. Boukhemacha, C. R. Gogu, I. Serpescu, D. Gaitanaru, and I. Bica, "A hydrogeological conceptual approach to study urban groundwater flow in Bucharest city, Romania," *Hydrogeology Journal*, vol. 23, no. 3, pp. 437–450, 2015.

[32] R. Ducommun, *Estimation et cartographie de la vulnérabilité des eaux souterraines en milieu urbain(Estimation and mapping of groundwater vulnerability in urban areas)*, Université de Neuchâtel, Switzerland, Europe, 2010.

[33] G. Attard, T. Winiarski, Y. Rossier, and L. Eisenlohr, "Review: impact of underground structures on the flow of urban groundwater," *Hydrogeology Journal*, vol. 24, no. 1, pp. 5–19, 2015.

[34] L. Liu, M. Lei, C. Cao, and C. Shi, "Dewatering characteristics and inflow prediction of deep foundation pits with partial penetrating curtains in sand and gravel strata," *Water*, vol. 11, no. 10, p. 2182, 2019a.

[35] E. Pujades, E. Vázquez-Suñé, L. Culí, J. Carrera, A. Ledesma, and A. Jurado, "Hydrogeological impact assessment by tunnelling at sites of high sensitivity," *Engineering Geology*, vol. 193, pp. 421–434, 2015.

[36] *ASTM International Standard Test Methods for Laboratory Determination of Density (Unit Weight) of Soil Specimens*, American Society for Testing Materials, West Conshohocken, PA, US, 2009.

[37] T. W. Lambe and Whitman, *Soil Mechanics*, Wiley, 1991.